Supplementary Information

Ultra-high piezo-photocatalytic performance of (Na, Sm) co-doped $CaBi_2Nb_2O_9$ nanoplates by surface effect

Qiuyan Yi, Xiaogang Luo, Xuefan Zhou, Yan Zhao, Qiong Liu, Qiwei Sun, Hang Luo, Dou Zhang**

State Key Laboratory of Powder Metallurgy, Central South University, Changsha, Hunan 410083, China

***Corresponding author**

E-mail address:

hangluo@csu.edu.cn (Hang Luo)

dzhang@csu.edu.cn (Dou Zhang)

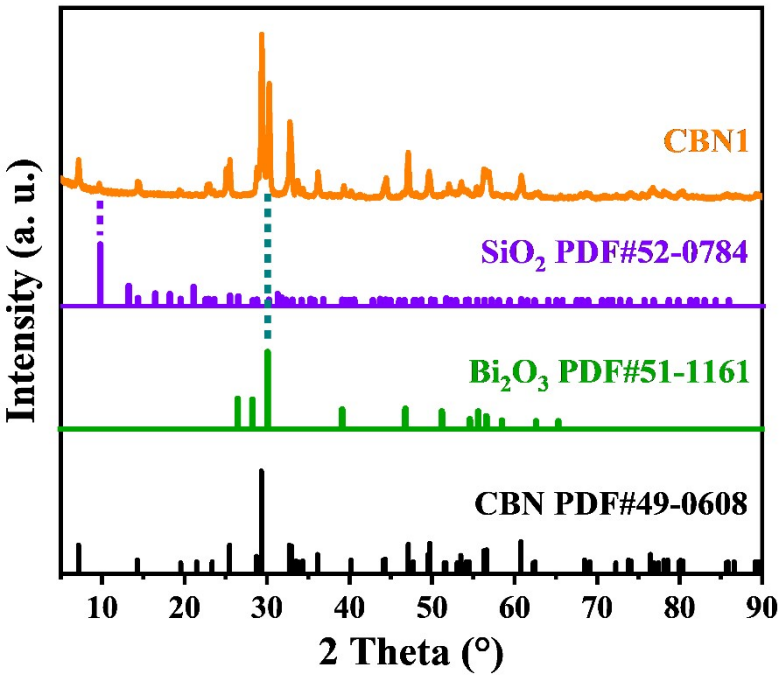

Figure S1 XRD pattern of CBN1.

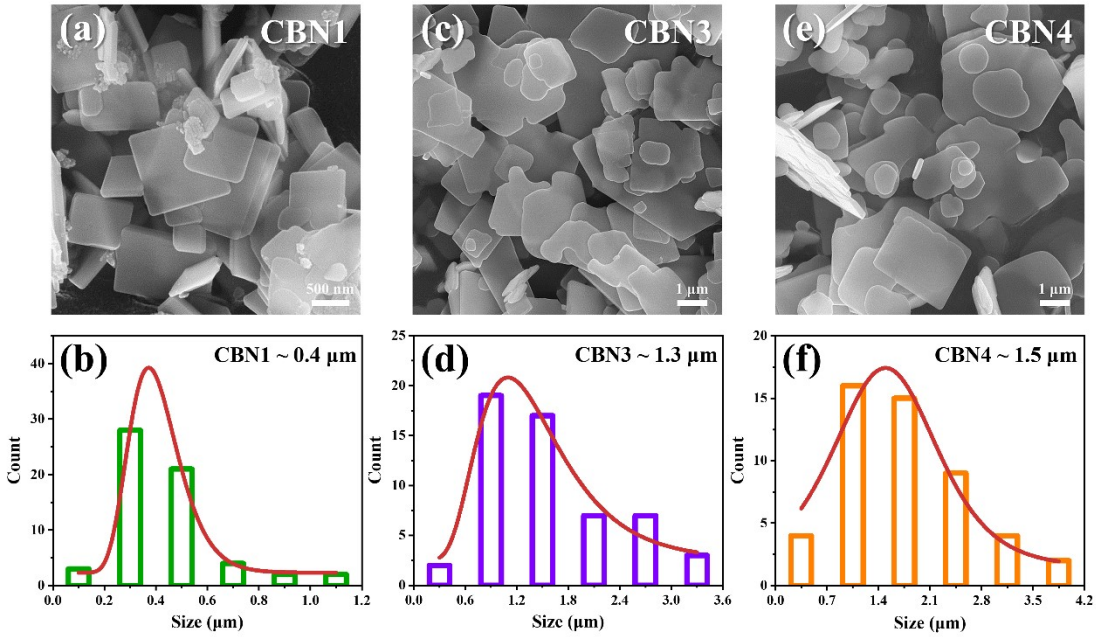

Figure S2 SEM images of a) CBN1, c) CBN3, and e) CBN4. Distribution maps of grain sizes of b) CBN1, d) CBN3, and f) CBN4.

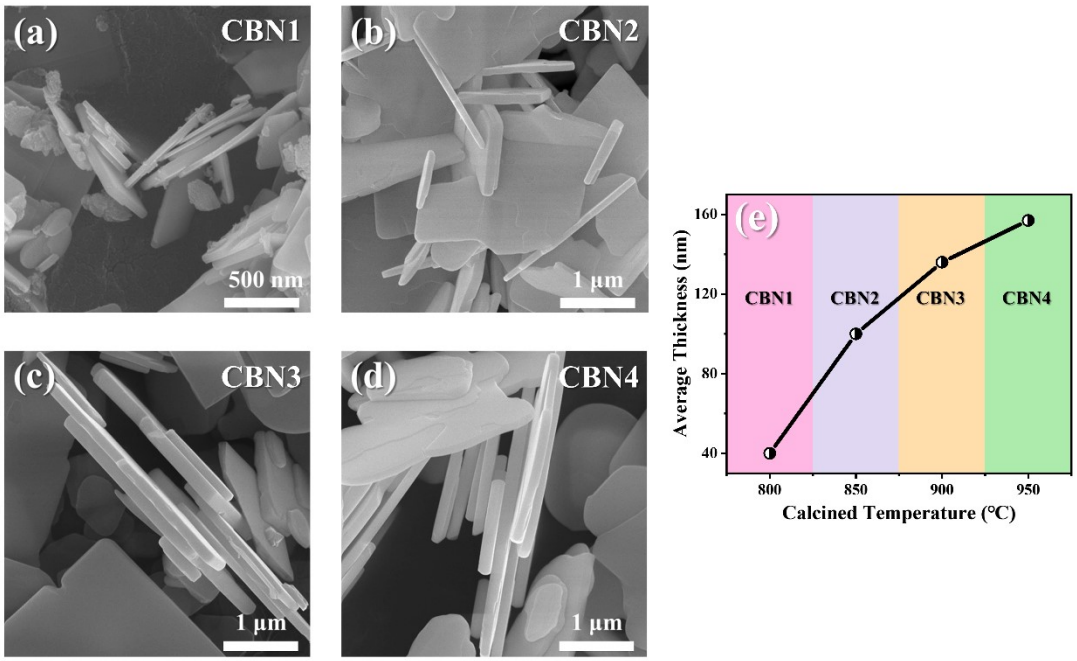

Figure S3 SEM images focusing on the thickness of a) CBN1, b) CBN2, c) CBN3, and d) CBN4. e) The increasing average thickness with the calcined temperature.

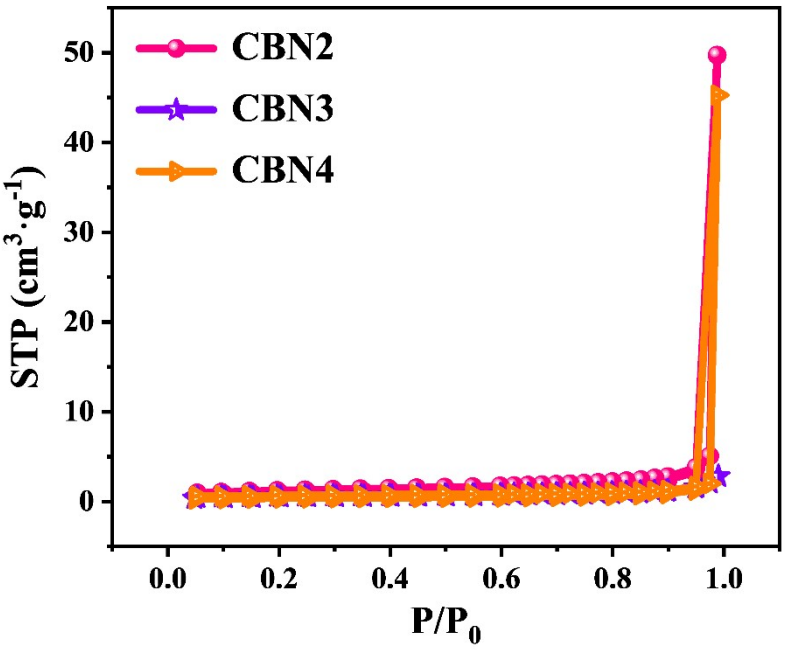

Figure S4 N_2 isothermal adsorption curves of CBN2, CBN3, and CBN4.

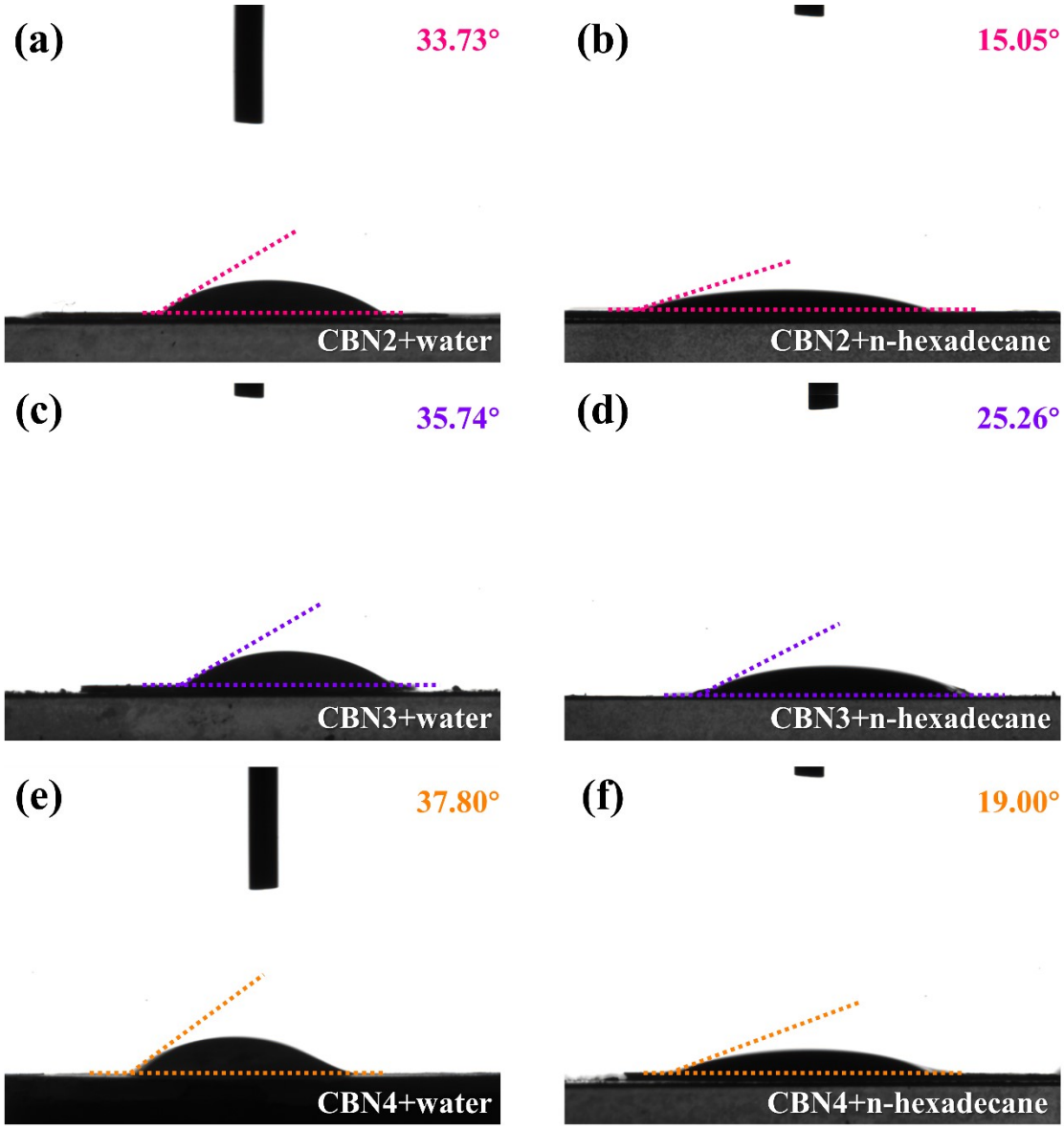

Figure S5 Contact angles of a) CBN2, c) CBN3, and e) CBN4 on water, b) CBN2, d) CBN3, and f) CBN4 on n-hexadecane.

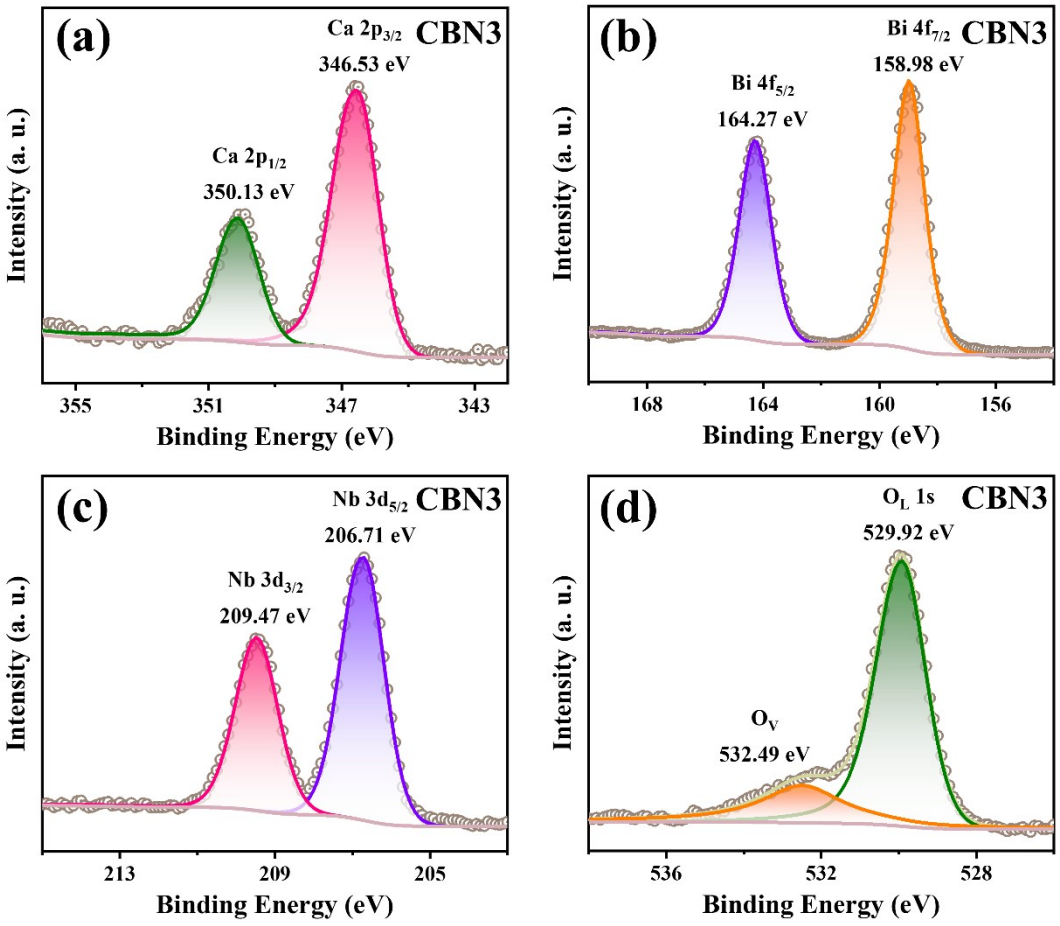

Figure S6 XPS spectra of a) Ca 2p, b) Bi 4f, c) Nb 3d, and d) O 1s of CBN3.

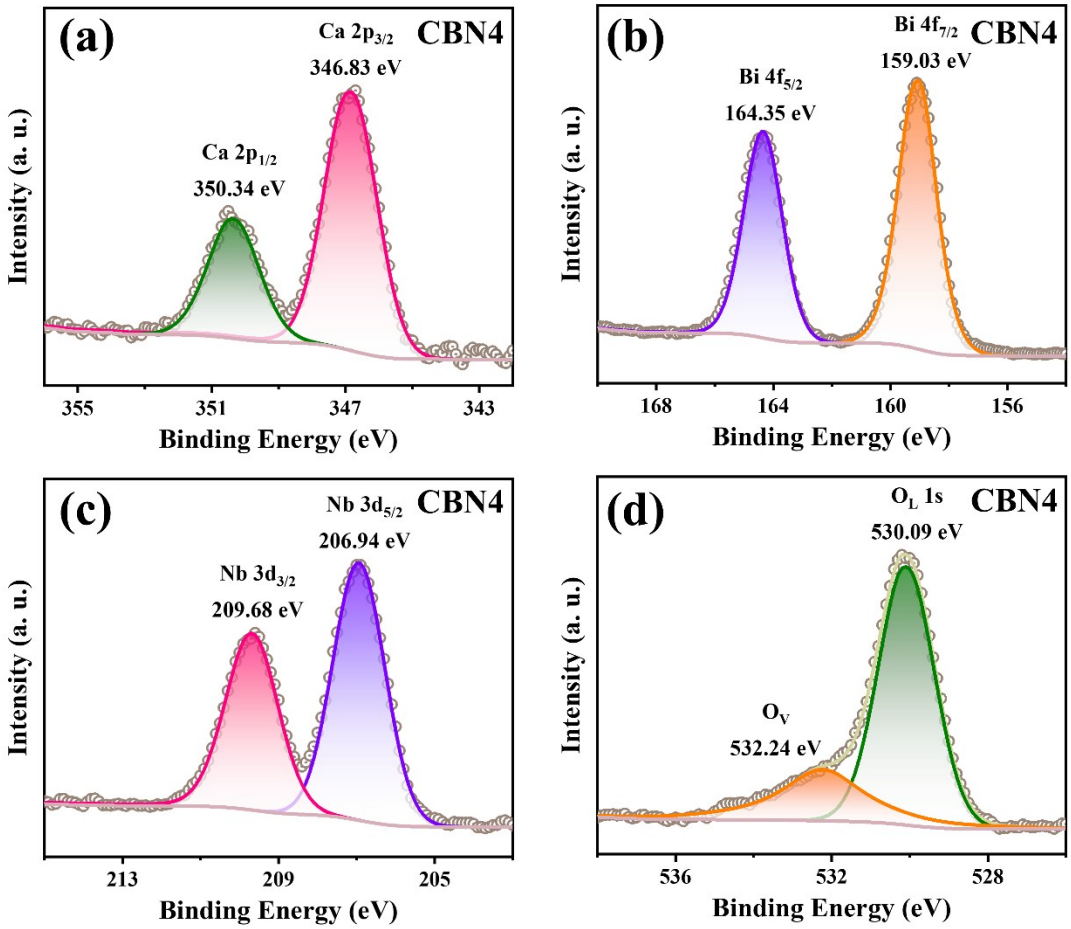

Figure S7 XPS spectra of a) Ca 2p, b) Bi 4f, c) Nb 3d, and d) O 1s of CBN4.

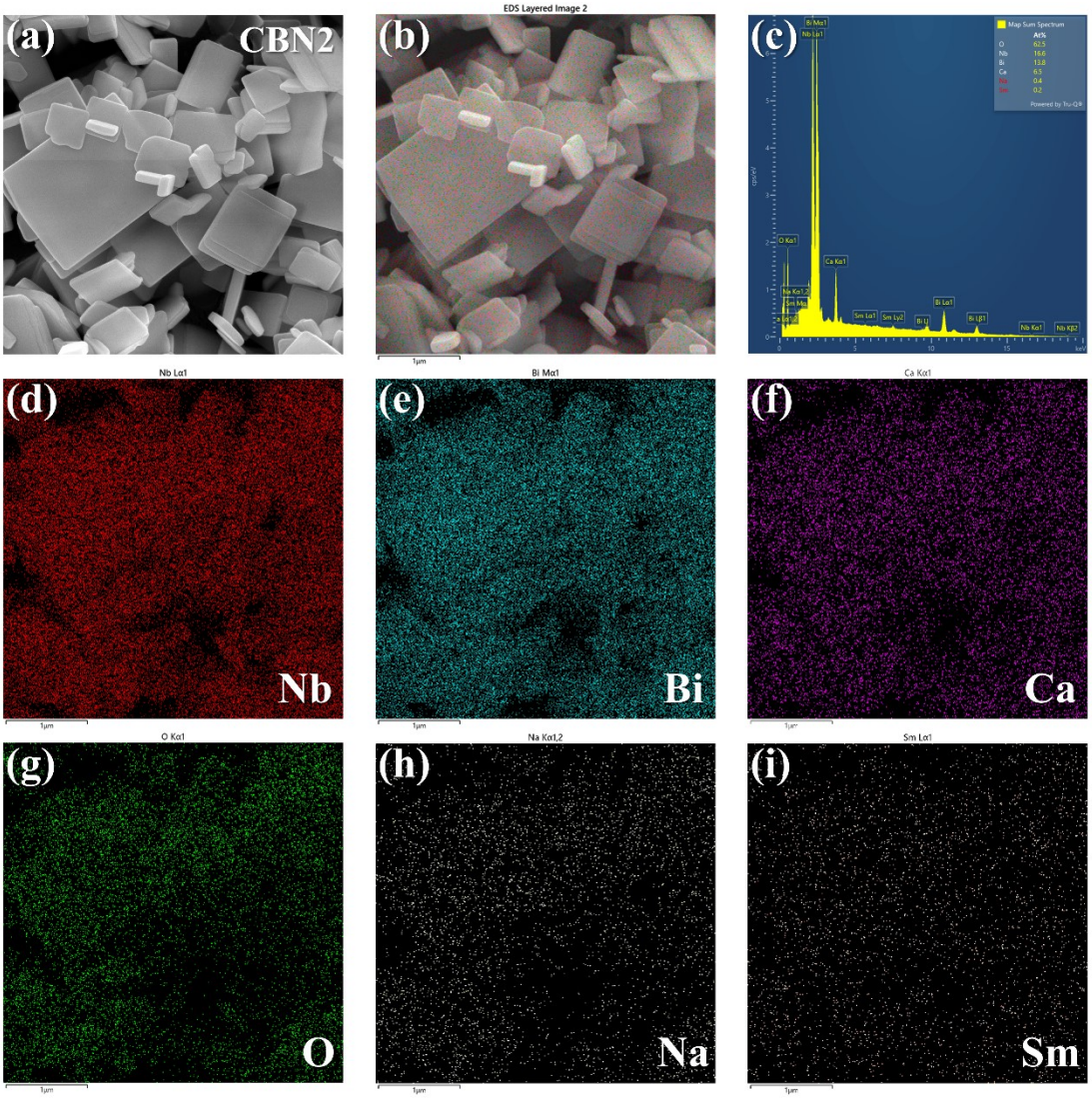

Figure S8 a) SEM image, b) EDS layered image, c) map sum spectrum, d) Nb, e) Bi, f) Ca, g) O, h) Na, and i) Sm of CBN2.

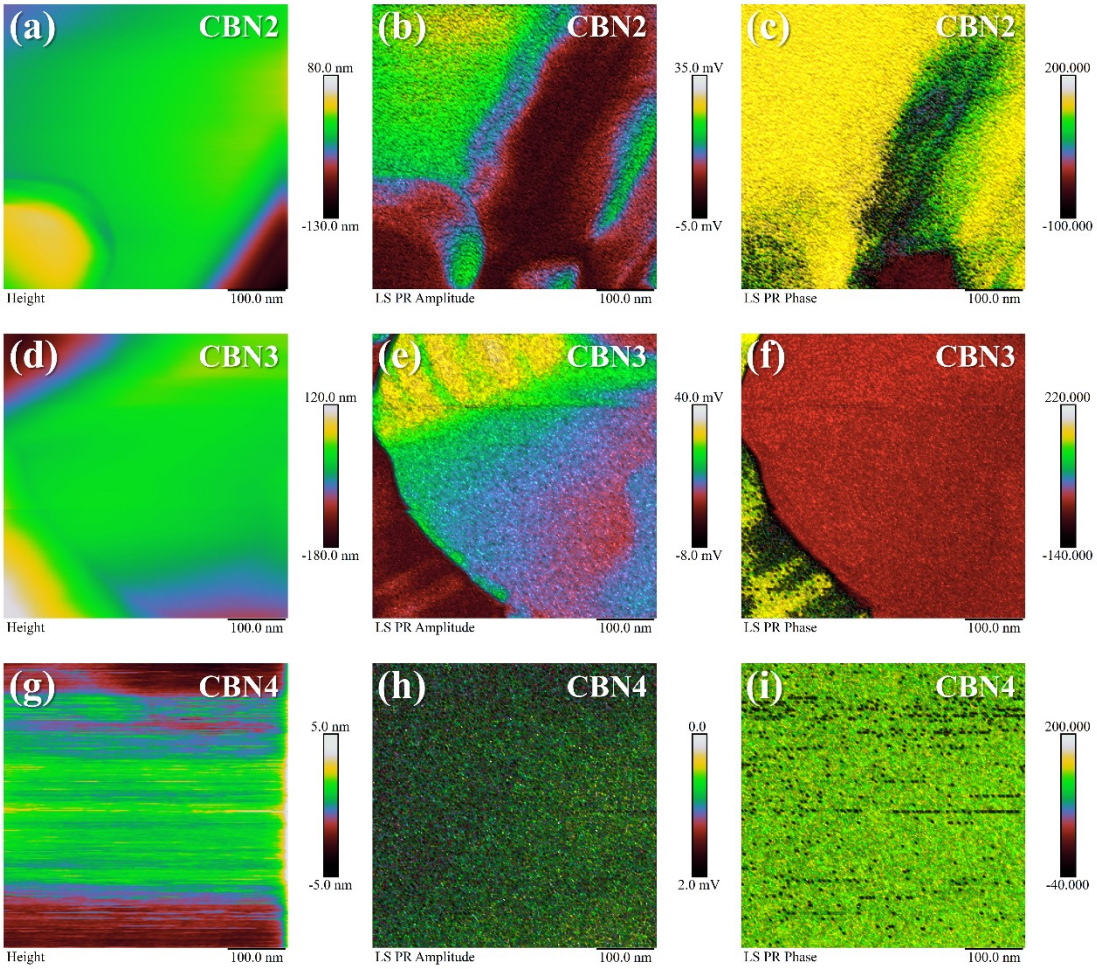

Figure S9 a) Morphological image, b) amplitude image, and c) phase image of CBN2. d) Morphological image, e) amplitude image, and f) phase image of CBN3, g) Morphological image, h) amplitude image, and i) phase image of CBN4.

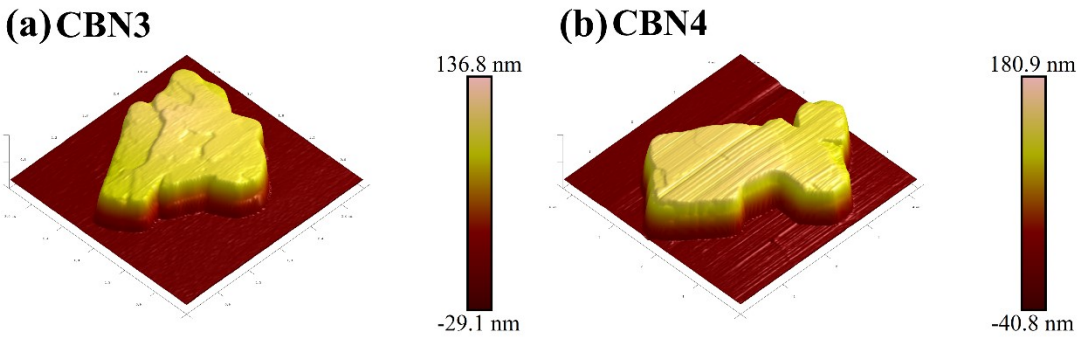

Figure S10 3D images of a) CBN3 and b) CBN4 by PFM.

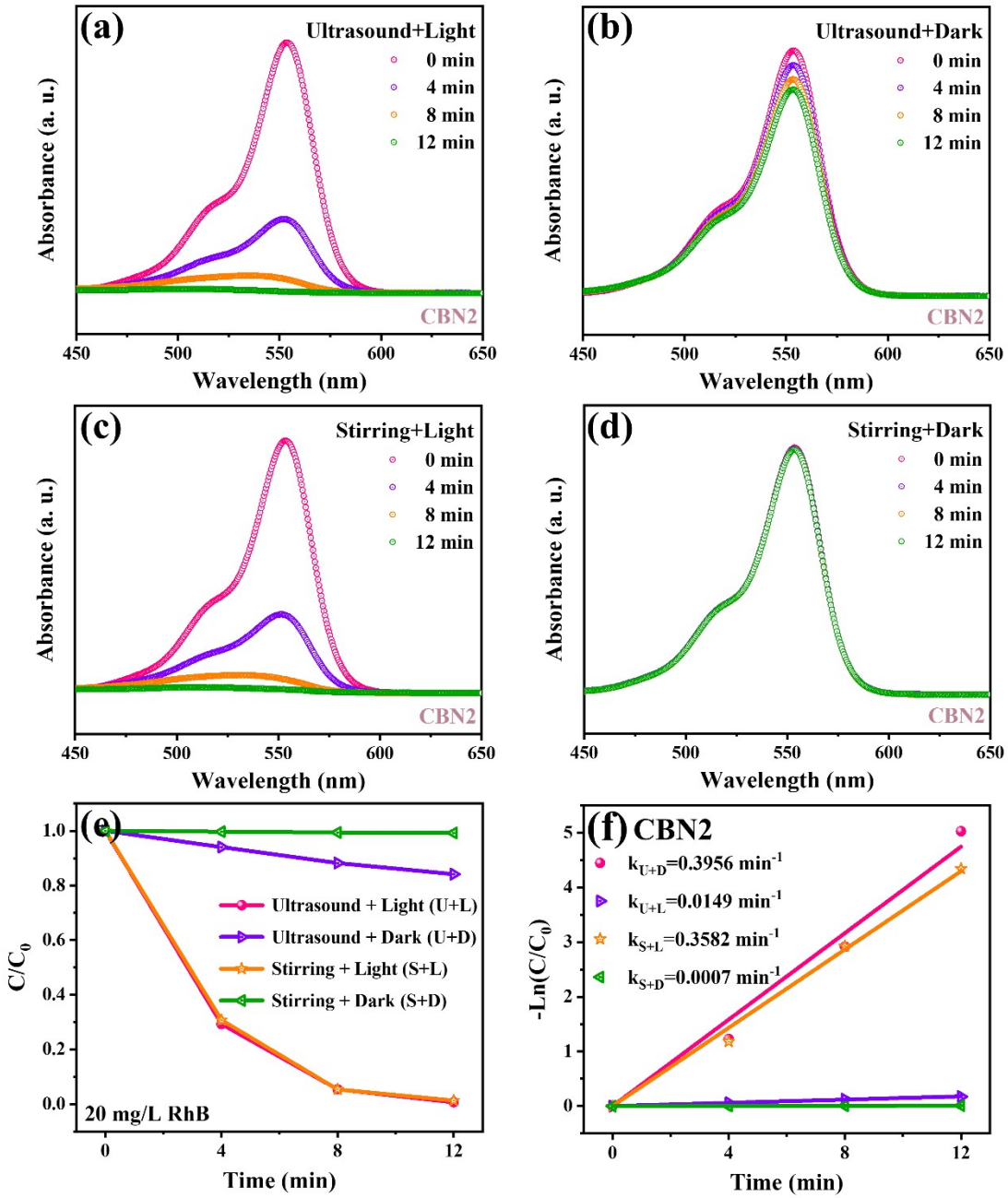

Figure S11 Piezo-photocatalytic performance on **20 mg·L^{-1} RhB by CBN2** under the following applied excitations: a) Ultrasound + Light, b) Ultrasound + Dark, c) Stirring + Light, and d) Stirring + Dark. Plots of e) C/C_0 and f) the fitted *k*-values versus reaction time.

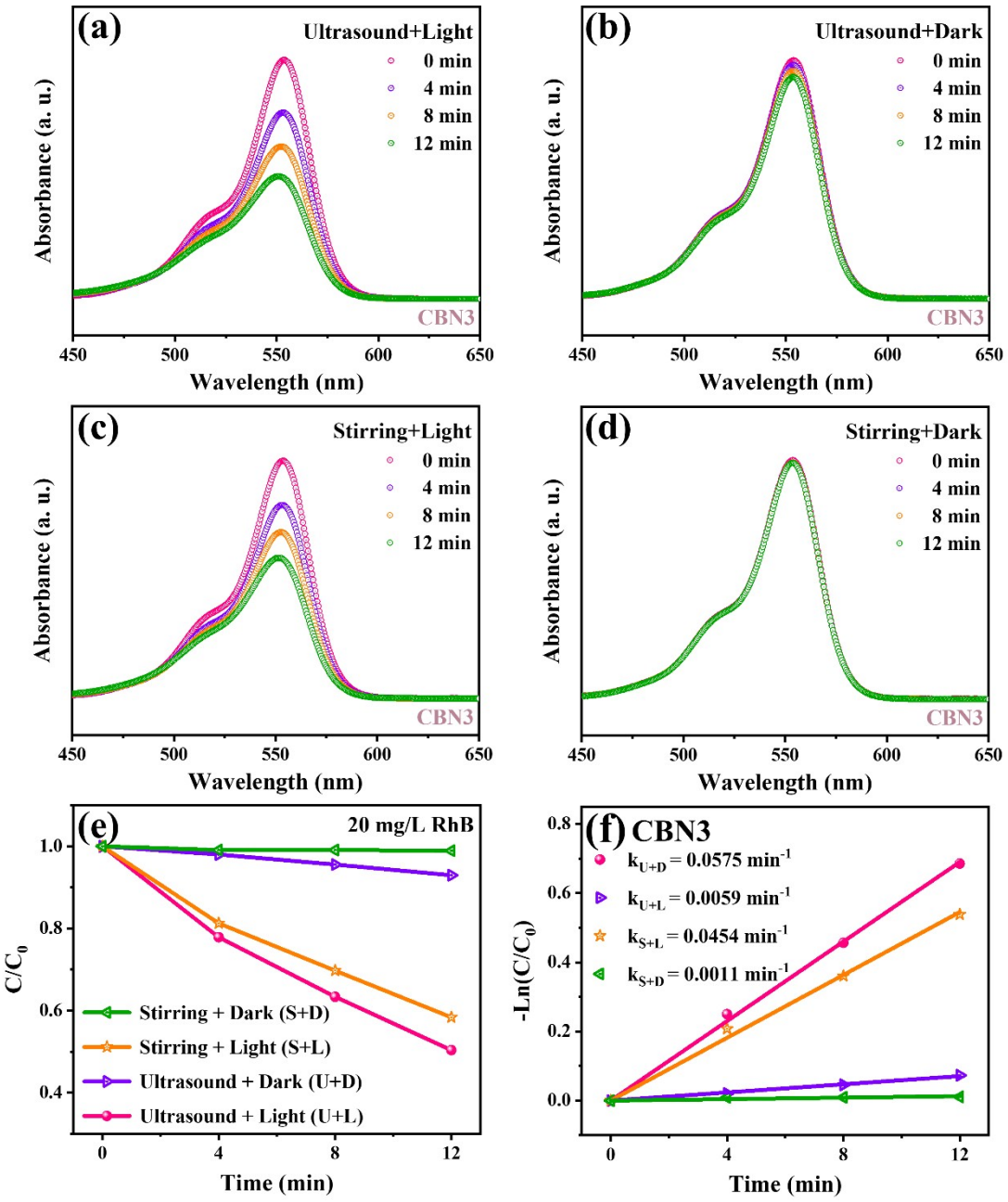

Figure S12 Piezo-photocatalytic performance on **20 mg·L^{-1} RhB by CBN3** under the following applied excitations: a) Ultrasound + Light, b) Ultrasound + Dark, c) Stirring + Light, and d) Stirring + Dark. Plots of e) C/C_0 and f) the fitted *k*-values versus reaction time.

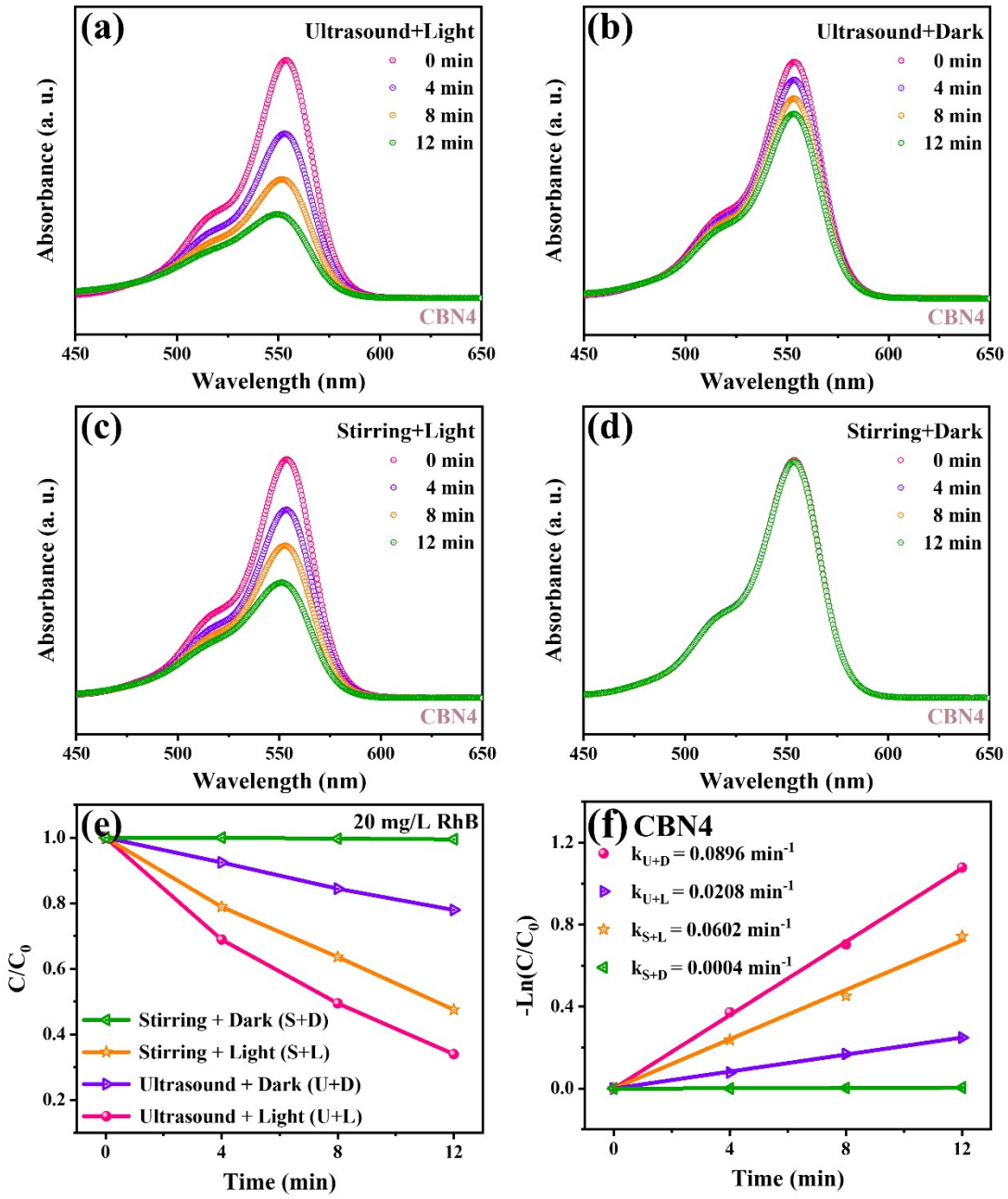

Figure S13 Piezo-photocatalytic performance on **20 mg·L^{-1} RhB by CBN4** under the following applied excitations: a) Ultrasound + Light, b) Ultrasound + Dark, c) Stirring + Light, and d) Stirring + Dark. Plots of e) C/C_0 and f) the fitted *k*-values versus reaction time.

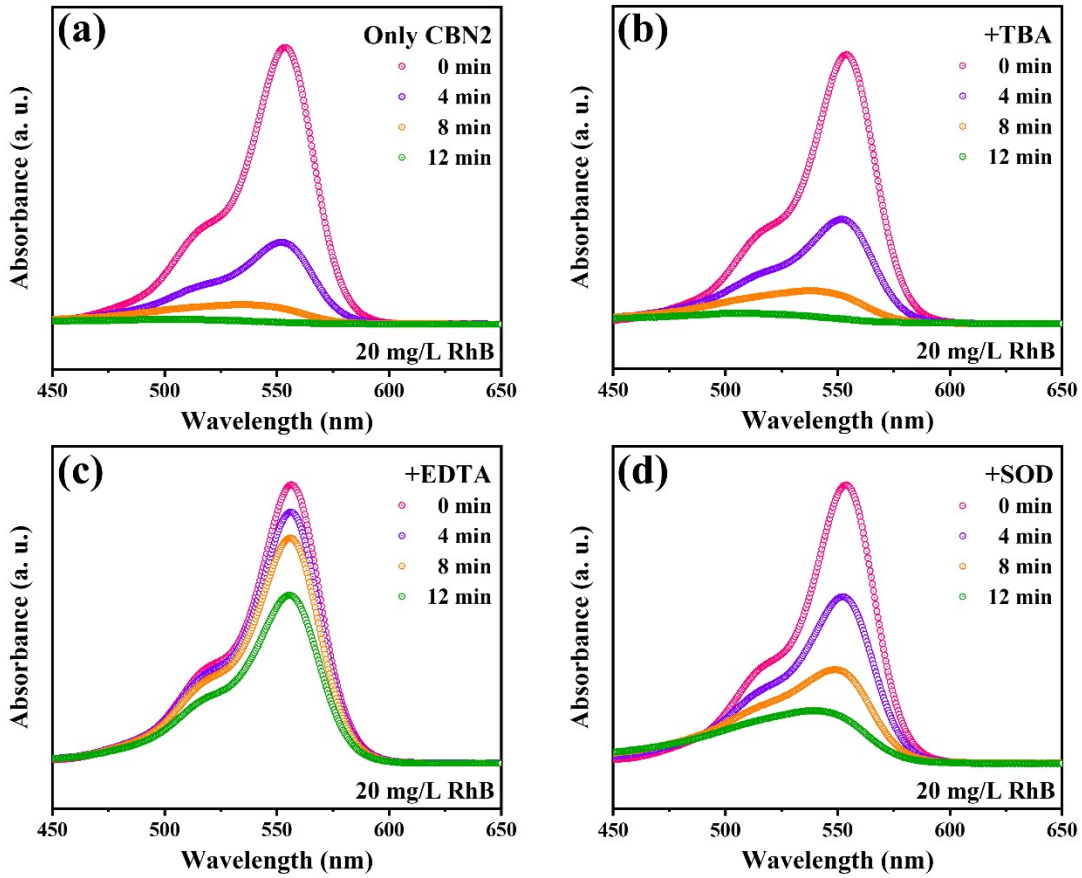

Figure S14 Piezo-photocatalytic curves on **20 mg·L^{-1} RhB by CBN2** with a) only catalysts, b) TBA, c) EDTA, and d) SOD added.

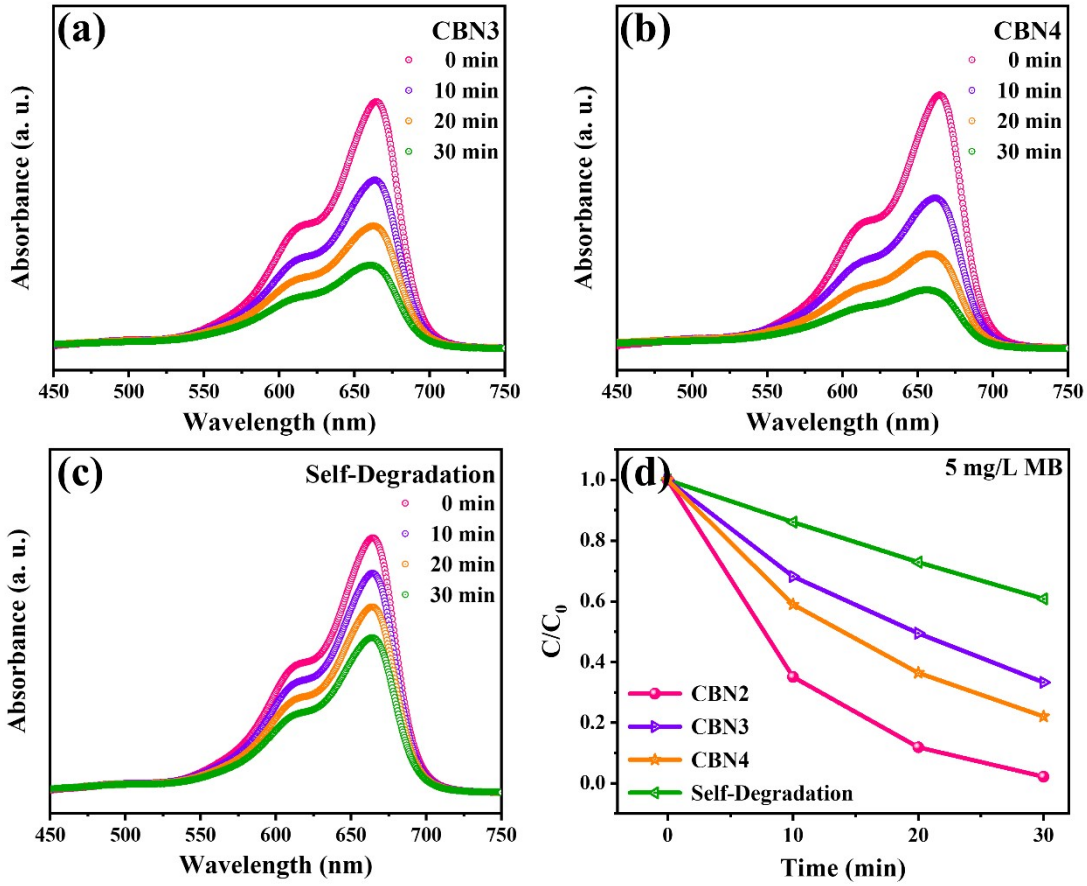

Figure S15 Piezo-photocatalytic performance on **5 mg·L^{-1} MB** by a) CBN3, b) CBN4, and c) self-degradation. d) Plots of C/C_0 versus reaction time.

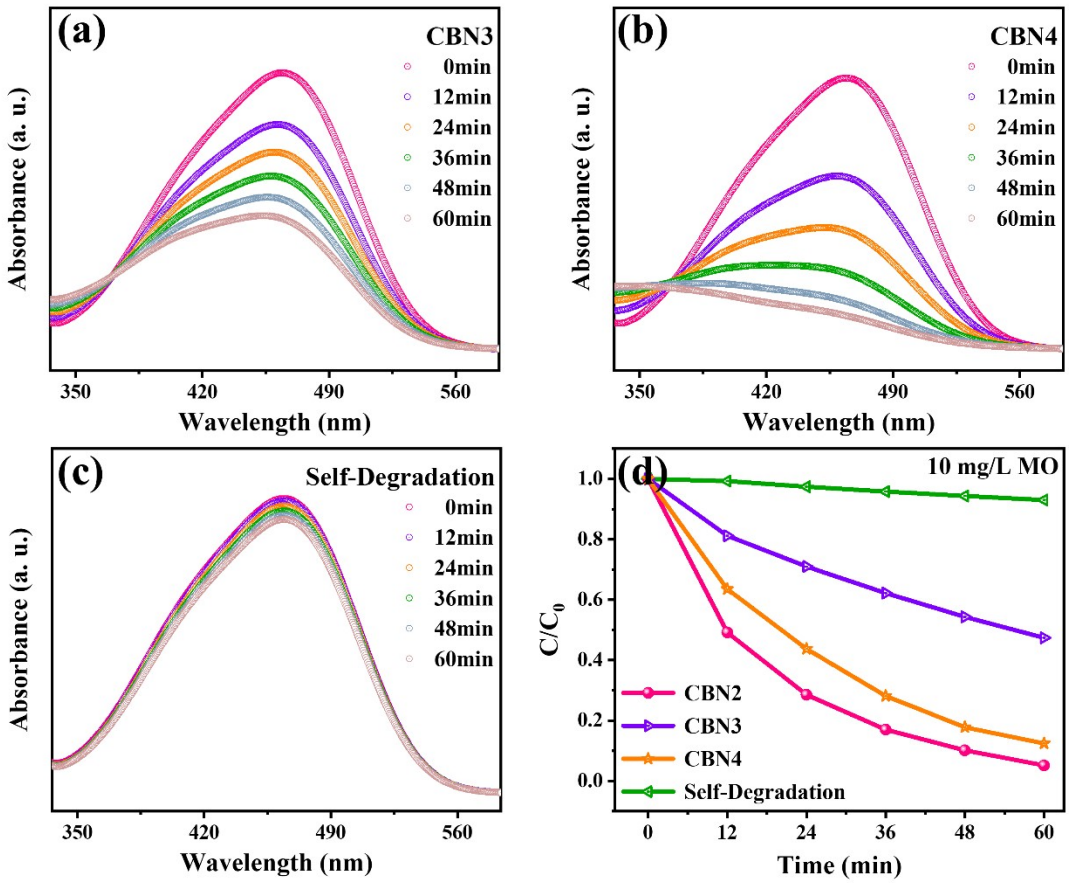

Figure S16 Piezo-photocatalytic performance on **10 mg·L^{-1} MO** by a) CBN3, b) CBN4, and c) self-degradation. d) Plots of C/C_0 versus reaction time.

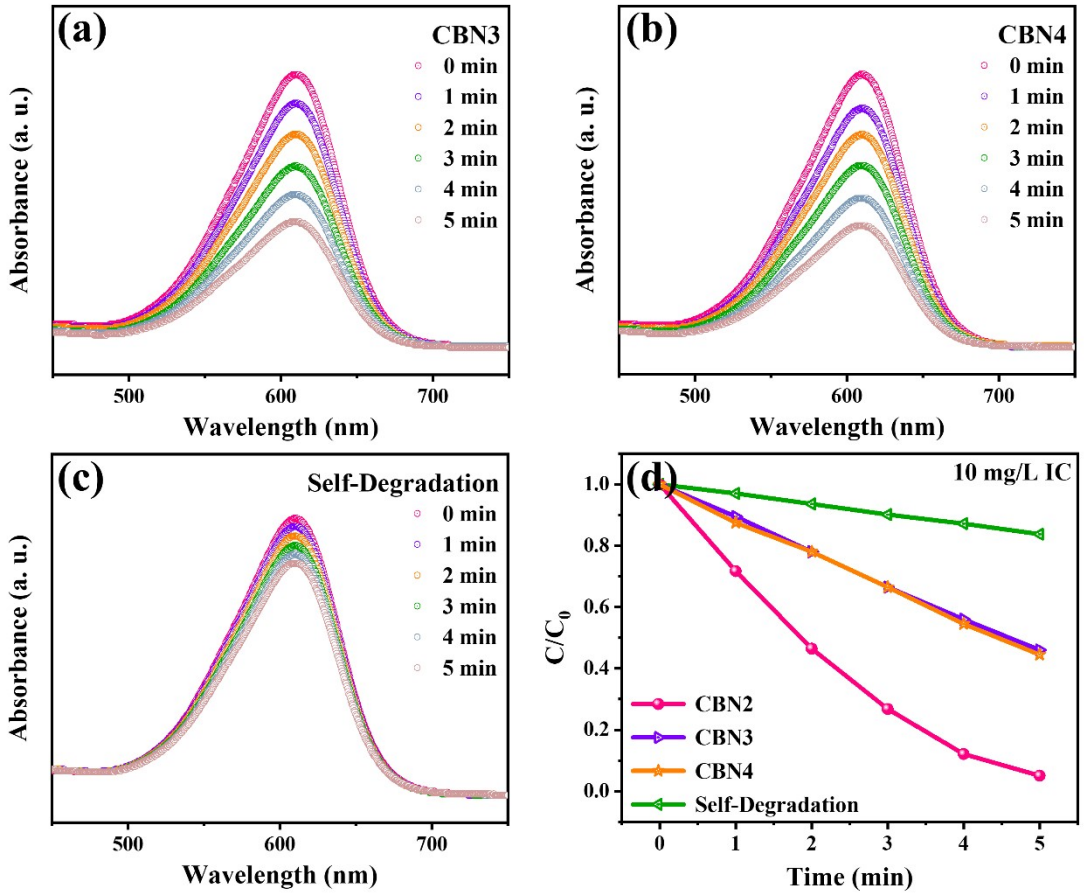

Figure S17 Piezo-photocatalytic performance on **10 mg·L^{-1} IC** by a) CBN3, b) CBN4, and c) self-degradation. d) Plots of C/C_0 versus reaction time.

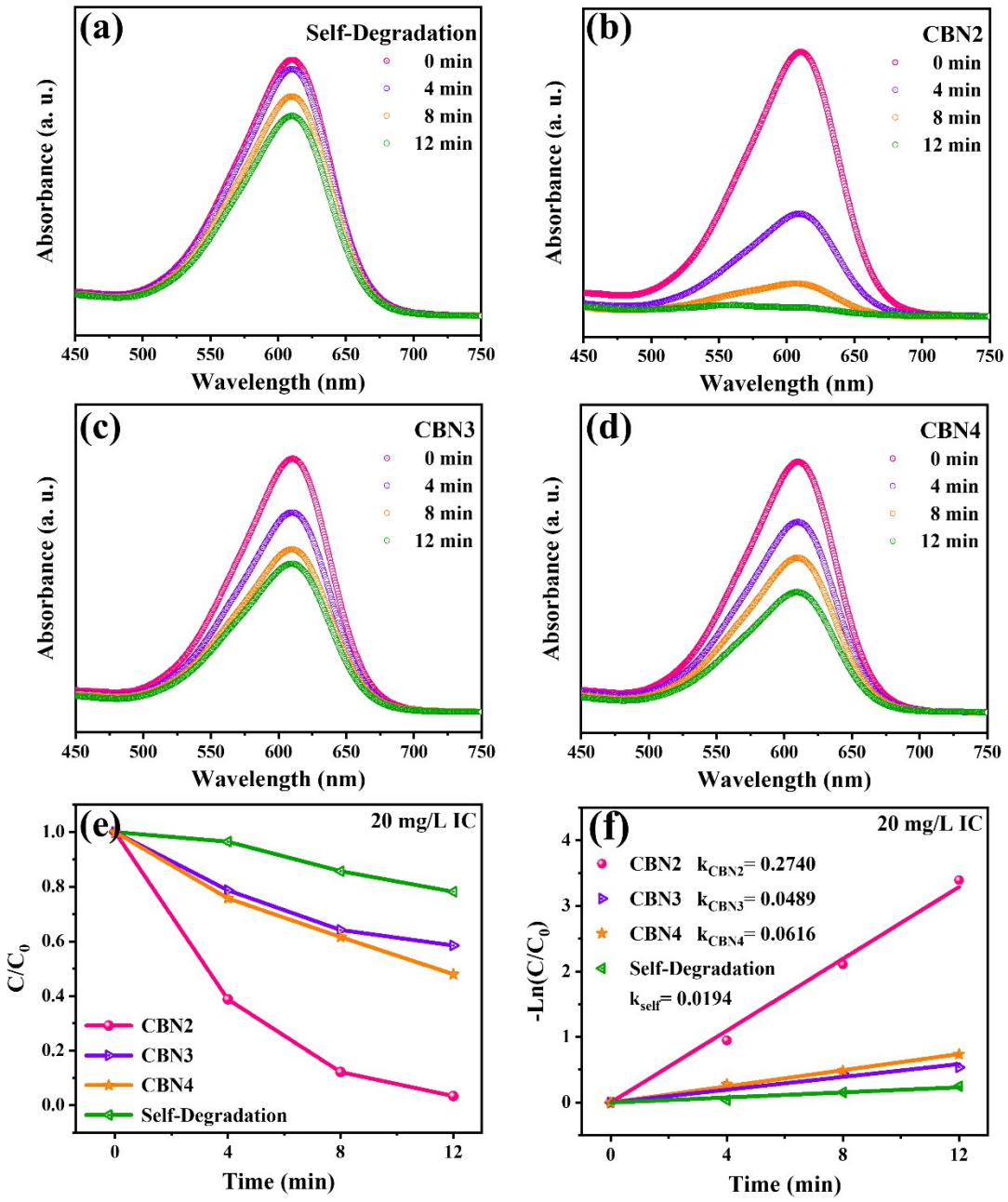

Figure S18 Piezo-photocatalytic performance on **20 mg·L^{-1} IC** by a) self-degradation, b) CBN2, c) CBN3, and d) CBN4. Plots of e) C/C_0 and f) the fitted *k*-values versus reaction time.

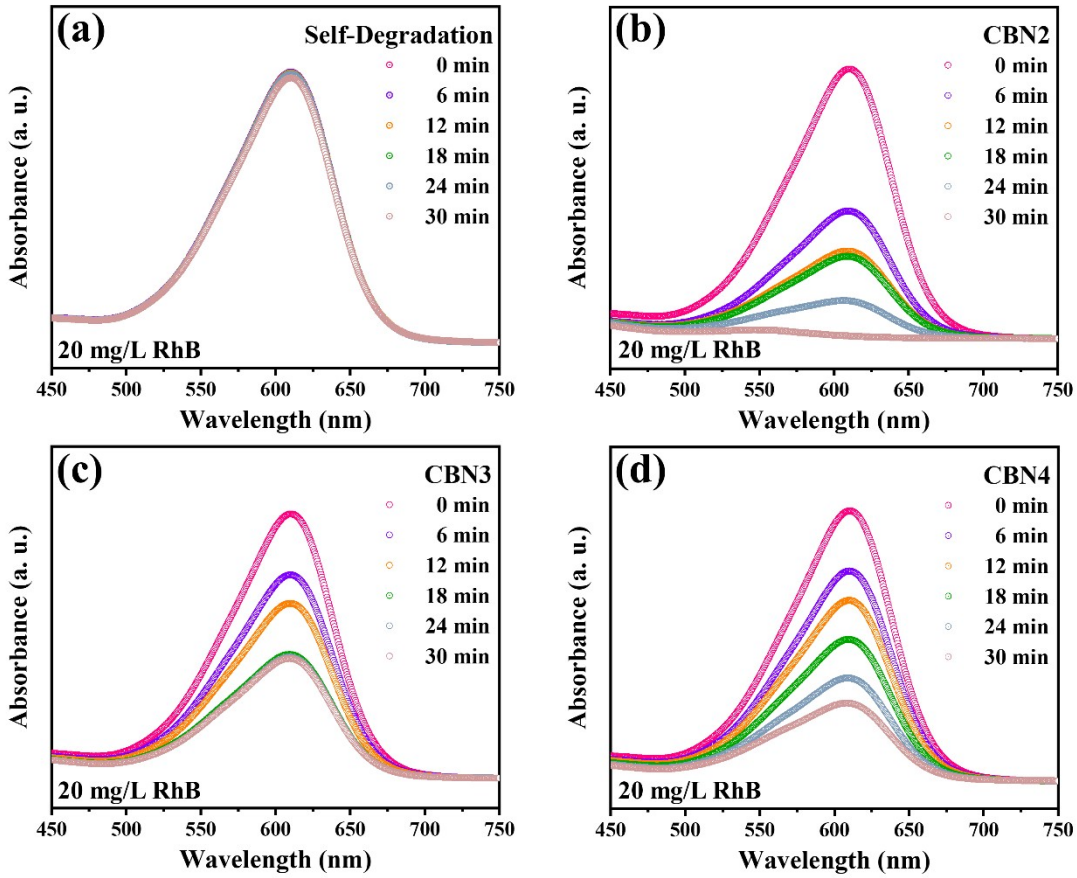

Figure S19 Piezo-photocatalytic performance on **50 mg·L^{-1} IC** by a) self-degradation, b) CBN2, c) CBN3, and d) CBN4.

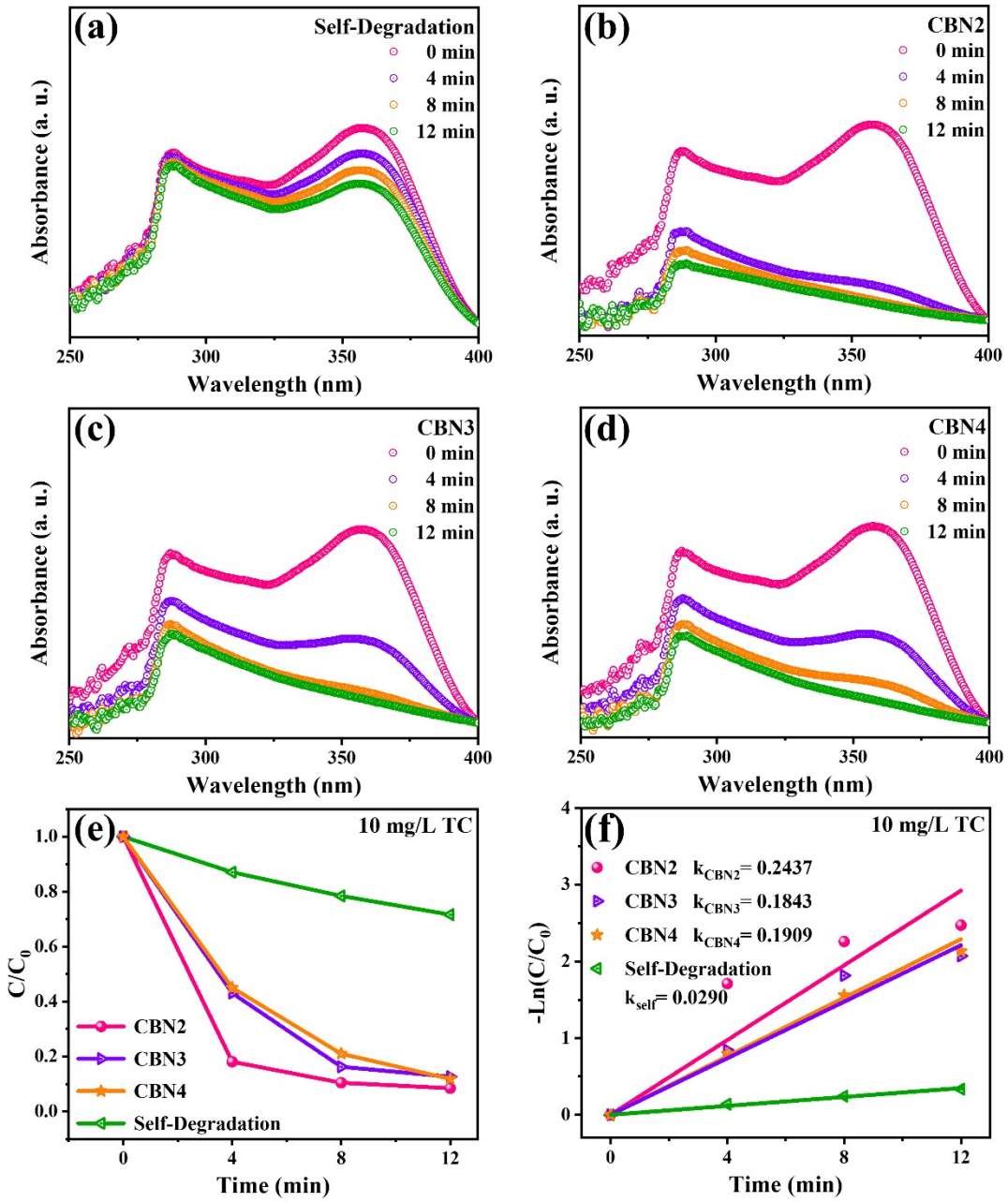

Figure S20 Piezo-photocatalytic performance on **10 mg·L^{-1} TC** by a) self-degradation, b) CBN2, c) CBN3, and d) CBN4. Plots of e) C/C_0 and f) the fitted *k*-values versus reaction time.

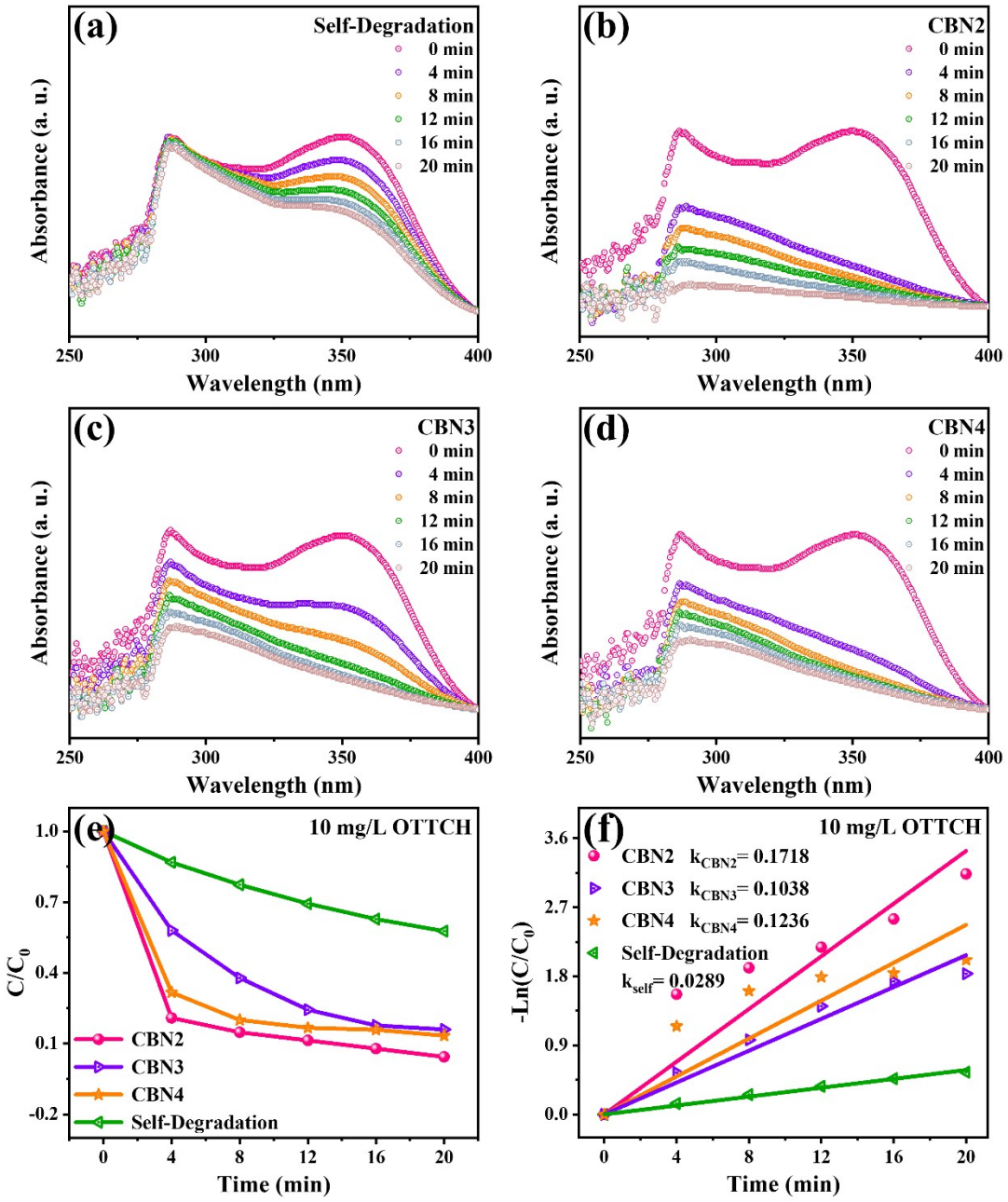

Figure S21 Piezo-photocatalytic performance on **10 mg·L^{-1} OTTCH** by a) self-degradation, b) CBN2, c) CBN3, and d) CBN4. Plots of e) C/C_0 and f) the fitted *k*-values versus reaction time.

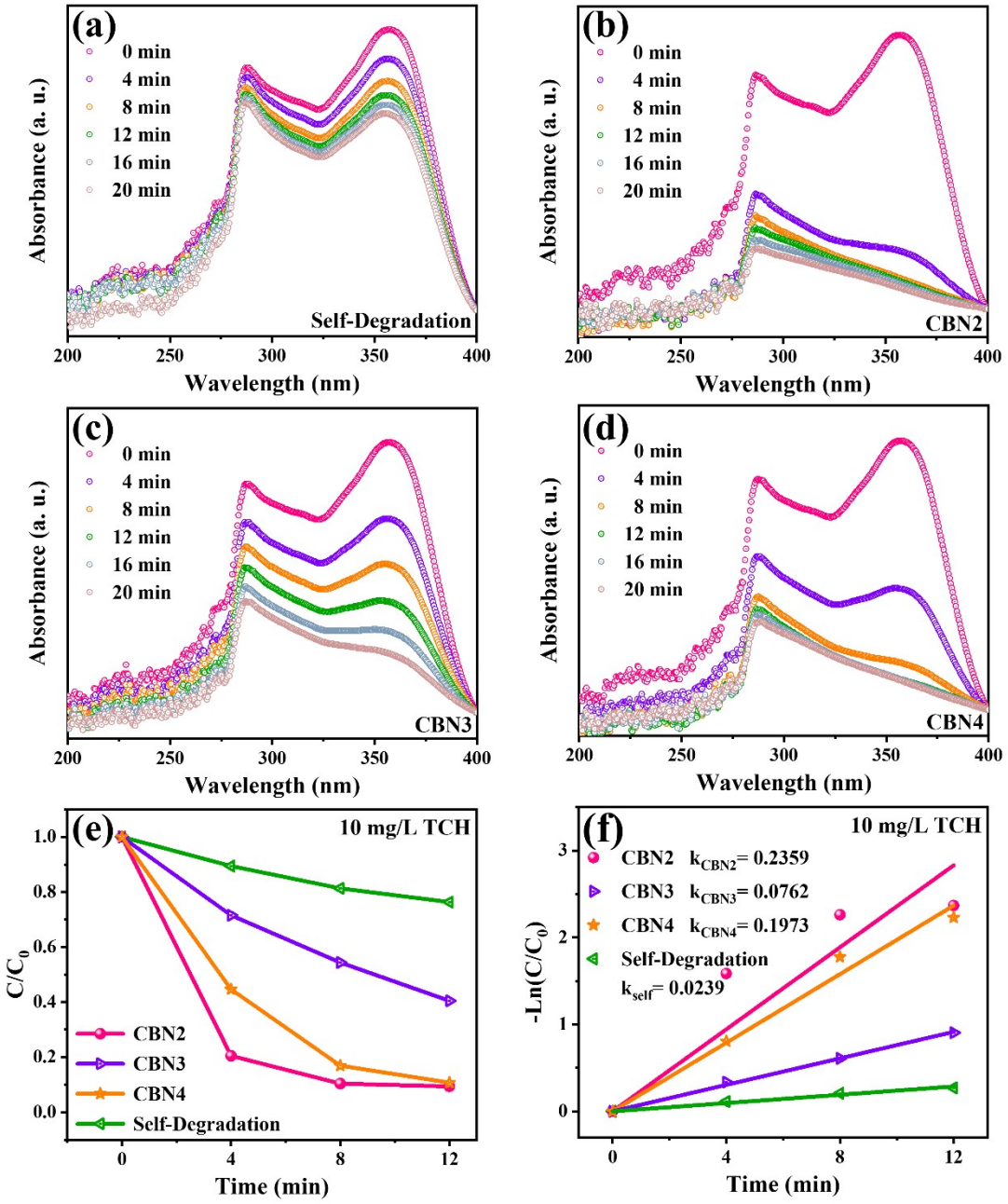

Figure S22 Piezo-photocatalytic performance on **10 mg·L^{-1} TCH** by a) self-degradation, b) CBN2, c) CBN3, and d) CBN4. Plots of e) C/C_0 and f) the fitted *k*-values versus reaction time.

Table S1 Contents of the elements in CBN2 obtained by EDS.

Element	Signal Type	Wt%
O	EDS	17.44
Na	EDS	0.17
Ca	EDS	4.52
Nb	EDS	26.98
Sm	EDS	0.40
Bi	EDS	50.49
Total		**100.00**

Table S2 Fitted results of Nyquist plots.

Samples	Ohmic Resistance	Transfer Resistance
CBN2	13.89	85461
CBN3	16.93	315100
CBN4	14.55	134860

Table S3 Fitted *k*-values of recently reported piezo-photocatalysis.

catalyst	$C_{(catalyst)}$	$C_{(Dye)}$	Condition	Year	$k\times10^{-3}$ (min^{-1})	Ref
$BaTiO_3$-O_Vs nanoparticles	1 $g\cdot L^{-1}$	10 $mg\cdot L^{-1}$ RhB	Ultrasonic: 300 W, 40 kHz Xenon lamp: 300 W	2023	34.1	[1]
$NaNbO_3/WO_3$	0.25 $g\cdot L^{-1}$	10 $mg\cdot L^{-1}$ RhB	Ultrasonic: 180 W, 40 kHz Xenon lamp: 300 W	2023	10.7	[2]
$Bi_{0.5}Na_{0.5}TiO_3$	1 $g\cdot L^{-1}$	5 $mg\cdot L^{-1}$ RhB	Ultrasonic: 200 W, 40 kHz Xenon lamp: 300 W	2022	167	[3]
$BiOCl/NaNbO_3$	1 $g\cdot L^{-1}$	5 $mg\cdot L^{-1}$ RhB	Ultrasonic: 50 W, 40 kHz Xenon lamp: 300 W	2022	19.2	[4]
$Ag@Na_{0.5}Bi_{0.5}TiO_3$	1 $g\cdot L^{-1}$	5 $mg\cdot L^{-1}$ RhB	Ultrasonic: 300 W, 40 kHz Xenon lamp: 300 W	2022	146	[5]
$AgCl/BiFeO_3$	0.5 $g\cdot L^{-1}$	10 $mg\cdot L^{-1}$ RhB	Xenon lamp: 300 W	2024	13.07	[6]
(Na^+, Sm^{3+}) co-doped $CaBi_2Nb_2O_9$	0.5 $g\cdot L^{-1}$	10 $mg\cdot L^{-1}$ RhB	Ultrasonic: 200 W, 45 kHz Xenon lamp: 300 W	2024	773.4	This work
(Na^+, Sm^{3+}) co-doped $CaBi_2Nb_2O_9$	0.5 $g\cdot L^{-1}$	20 $mg\cdot L^{-1}$ RhB	Ultrasonic: 200 W, 45 kHz Xenon lamp: 300 W	2024	395.6	This work
$BiVO_4$ nanorods	0.33 $g\cdot L^{-1}$	2 $mg\cdot L^{-1}$ MB	Ultrasonic: 140 W, 35 kHz LED bulb: 20 W	2022	100	[7]
$Bi_2VO_{5.5}$	10 $g\cdot L^{-1}$	5 $mg\cdot L^{-1}$ MB	Ultrasonic: 120 W, 40 kHz Two bulbs: 15 W each	2023	5.29	[8]
$PVDF/CaNO_3$	/	2.5 $mg\cdot L^{-1}$ MB	Ultrasonic: 250 W, 18 kHz Mercury lamp: 250 W	2023	83	[9]
$KNbO_3/MoS_2$	1 $g\cdot L^{-1}$	10 ppm MB	Ultrasonic: 120 W, 40 kHz Mercury lamp: 300 W	2023	10.17	[10]
(Na^+, Sm^{3+}) co-	0.5 $g\cdot L^{-1}$	5 $mg\cdot L^{-1}$	Ultrasonic: 200 W, 45 kHz	2024	120.1	This

doped $CaBi_2Nb_2O_9$		MB	Xenon lamp: 300 W			work
ZnO/MoS_2	/	10 $mg·L^{-1}$ MO	Stirring: 1000 rmp Xe lamp: 300 W	2021	59	[11]
ZnO-S	1 $g·L^{-1}$	50 $mg·L^{-1}$ MO	Ultrasonic: 200 W, 40 kHz Mercury lamp: 300 W	2021	19	[12]
$BaTiO_3/CuO$	1 $g·L^{-1}$	10 $mg·L^{-1}$ MO	Ultrasonic Mercury lamp: 200 W	2022	50	[13]
$Cu@Na_{0.5}Bi_{4.5}Ti_4O_{15}$	1 $g·L^{-1}$	10 $mg·L^{-1}$ MO	Stirring Mercury lamp: 300 W	2022	24.67	[14]
(Na^+, Sm^{3+}) co-doped $CaBi_2Nb_2O_9$	0.5 $g·L^{-1}$	10 $mg·L^{-1}$ MO	Ultrasonic: 200 W, 45 kHz Xenon lamp: 300 W	2024	49.3	This work
$BaTiO_3$ nanoparticles	0.5 $g·L^{-1}$	10 $mg·L^{-1}$ IC	Ultrasonic: 200 W, 45 kHz Xenon lamp: 300 W	2023	99	[15]
$BaTiO_3@TiO_2$	0.5 $g·L^{-1}$	10 $mg·L^{-1}$ IC	Ultrasonic: 200 W, 45 kHz Xenon lamp: 300 W	2021	108	[16]
(Na^+, Sm^{3+}) co-doped $CaBi_2Nb_2O_9$	0.5 $g·L^{-1}$	10 $mg·L^{-1}$ IC	Ultrasonic: 200 W, 45 kHz Xenon lamp: 300 W	2024	530.7	This work
(Na^+, Sm^{3+}) co-doped $CaBi_2Nb_2O_9$	0.5 $g·L^{-1}$	20 $mg·L^{-1}$ IC	Ultrasonic: 200 W, 45 kHz Xenon lamp: 300 W	2024	274.0	This work
(Na^+, Sm^{3+}) co-doped $CaBi_2Nb_2O_9$	0.5 $g·L^{-1}$	50 $mg·L^{-1}$ IC	Ultrasonic: 200 W, 45 kHz Xenon lamp: 300 W	2024	115.3	This work

References

(1) Xiao, Q.; Chen, L.; Xu, Y.; Feng, W.; Qiu, X. Impact of oxygen vacancy on piezo-photocatalytic catalytic activity of barium titanate. *Applied Surface Science* **2023**, *619*, 156794. DOI: https://doi.org/10.1016/j.apsusc.2023.156794.

(2) Yan, X.; Zhang, S.; Pan, L.; Ai, T.; Li, Z.; Niu, Y. Synergetic piezo-photocatalytic effect in $NaNbO_3/WO_3$ photocatalyst for RhB degradation. *Inorganic Chemistry Communications* **2023**, *158*, 111510. DOI: https://doi.org/10.1016/j.inoche.2023.111510.

(3) Zhou, X.; Sun, Q.; Xiao, Z.; Luo, H.; Zhang, D. Three-dimensional BNT/PVDF composite foam with a hierarchical pore structure for efficient piezo-photocatalysis. *Journal of Environmental Chemical Engineering* **2022**, *10* (5). DOI: 10.1016/j.jece.2022.108399.

(4) Li, L.; Cao, W.; Yao, J.; Liu, W.; Li, F.; Wang, C. Synergistic piezo-photocatalysis of $BiOCl/NaNbO_3$ heterojunction piezoelectric composite for high-efficient organic pollutant degradation. In *Nanomaterials*, 2022; Vol. 12.

(5) Shi, J.; Xie, Z.; Tang, X.; Wang, Y.; Yuan, G.; Liu, J.-M. Enhanced piezo-photocatalytic performance of $Ag@Na_{0.5}Bi_{0.5}TiO_3$ composites. *Journal of Alloys and Compounds* **2022**, *911*, 164885. DOI: https://doi.org/10.1016/j.jallcom.2022.164885.

(6) Xian, T.; Ma, X.; Sun, X.; Sun, C.; Wang, H.; Di, L.; Ma, K.; Yang, H. Construction of p-n type $AgCl/BiFeO_3$ heterojunction with promising photocatalytic and piezo-photocatalytic water purification. *Optical Materials* **2024**, *149*, 115054. DOI: https://doi.org/10.1016/j.optmat.2024.115054.

(7) Deka, S.; Devi, M. B.; Khan, M. R.; Keerthana; Venimadhav, A.; Choudhury, B. Piezo-photocatalytic and photocatalytic bismuth vanadate nanorods with antibacterial property. *ACS Applied Nano Materials* **2022**, *5* (8), 10724-10734. DOI: 10.1021/acsanm.2c02072.

(8) Kumar, M.; Vaish, R.; Kebaili, I.; Boukhris, I.; Kwang Benno Park, H.; Hwan Joo, Y.; Hyun Sung, T.; Kumar, A. Ball-milling synthesized $Bi_2VO_{5.5}$ for piezo-photocatalytic assessment. *Scientific Reports* **2023**, *13* (1), 8188. DOI: 10.1038/s41598-023-33658-2.

(9) Orudzhev, F. F.; Sobola, D. S.; Ramazanov, S. M.; Částková, K.; Selimov, D. A.; Rabadanova, A. A.; Shuaibov, A. O.; Gulakhmedov, R. R.; Abdurakhmanov, M. G.; Giraev, K. M. Hydrogen bond-induced activation of photocatalytic and piezophotocatalytic properties in calcium nitrate doped electrospun PVDF fibers. *Polymers* **2023**, *15* (15), 3252.

(10) Ma, W.; Du, M.; Li, H.; Wang, Y.; Han, Z.; Chen, C.; Zhang, S.; Han, Q.; Li, Y.; Fang, J.; et al. The binary piezoelectric synergistic effect of $KNbO_3/MoS_2$ heterojunction for improving photocatalytic performance. *Journal of Alloys and Compounds* **2023**, *960*, 170669. DOI: https://doi.org/10.1016/j.jallcom.2023.170669.

(11) Fu, Y.; Ren, Z.; Wu, J.; Li, Y.; Liu, W.; Li, P.; Xing, L.; Ma, J.; Wang, H.; Xue, X. Direct Z-scheme heterojunction of ZnO/MoS2 nanoarrays realized by flowing-induced piezoelectric field for enhanced sunlight photocatalytic performances. *Applied Catalysis B: Environmental* **2021**, *285*, 119785. DOI: https://doi.org/10.1016/j.apcatb.2020.119785.

(12) Yang, R.; Wu, Z.; Yang, Y.; Li, Y.; Zhang, L.; Yu, B. Understanding the origin of synergistic catalytic activities for ZnO based sonophotocatalytic degradation of methyl orange. *Journal of the Taiwan Institute of Chemical Engineers* **2021**, *119*, 128-135. DOI: https://doi.org/10.1016/j.jtice.2021.01.028.

(13) Yu, C.; Tan, M.; Tao, C.; Hou, Y.; Liu, C.; Meng, H.; Su, Y.; Qiao, L.; Bai, Y. Remarkably enhanced piezo-photocatalytic performance in $BaTiO_3/CuO$ heterostructures for organic pollutant degradation. *Journal of Advanced Ceramics* **2022**, *11* (3), 414-426. DOI: 10.1007/s40145-021-0544-4.

(14) Lan, S.; Zheng, M.; Wu, J.; Lv, H.; Gao, X.; Zhang, Y.; Zhu, M.; Hou, Y. Copper nanoparticles-modified $Na_{0.5}Bi_{4.5}Ti_4O_{15}$ micron-sheets as a highly efficient and low cost piezo-photocatalyst. *Journal of Alloys and Compounds* **2023**, *935*, 168130. DOI: https://doi.org/10.1016/j.jallcom.2022.168130.
(15) Yi, Q.; Luo, H.; Xiong, H.; Liu, Q.; Zhai, D.; Sun, Q.; Zhang, D. Enhanced catalytic activity of Molar-like $BaTiO_3$ by oxygen vacancies. *Ceramics International* **2023**, *49* (23, Part B), 39707-39718. DOI: https://doi.org/10.1016/j.ceramint.2023.09.332.
(16) Liu, Q.; Zhai, D.; Xiao, Z.; Tang, C.; Sun, Q.; Bowen, C. R.; Luo, H.; Zhang, D. Piezo-photoelectronic coupling effect of $BaTiO_3$@TiO_2 nanowires for highly concentrated dye degradation. *Nano Energy* **2022**, *92*, 106702. DOI: 10.1016/j.nanoen.2021.106702.